SPATIAL-TEMPORAL MAPPING OF THE IMPACT OF LAND USE CHANGES ON FOREST COVER AND CULTIVATED LAND IN AWKA: A KEY DRIVER OF CLIMATE CHANGE AND FOOD INSECURITY

RICHARD EBERE NJOKU[1], MFONISO ASUQUO ENOH[2]*, CHUKWUBUEZE ONWUZULIGBO[3], UGWUOTI AMOS ILOABUCHI[2] AND CHINAZA HENRY OBINEME[3]

[1]*Department of Surveying and Geoinformatics, Federal University of Technology, Owerri, Nigeria*
[2]*Department of Geoinformatics and Surveying, University of Nigeria, Enugu*
[3]*Department of Surveying and Geoinformatics, Nnamdi Azikiwe University, Awka, Nigeria*
**Corresponding author email: enohmfoniso@yahoo.com*

Received: 17th April 2025, **Accepted:** 4th September 2025

ABSTRACT

The study used remotely sensed tools to map the impact of land use changes on Awka's forest cover and cultivated land. These changes tend to impact the city's forest cover and cultivated land, leading to climate change and food insecurity. The UN SDGs 2 and 13 outline plans of action that must be followed in order to attain sustainability and mitigate against the effects of climate change and food insecurity.

The study aims to analyze the impact of land use changes on forest cover and cultivated land in Awka from 2010 to 2020.

In this study, three remotely sensed satellite data sets (Landsat 7 ETM+ 2010 and Landsat 8 OLI 2015, 2020) were used to map the impact of land use change on forest cover and cultivated land in Awka. The remote sensing techniques adopted were image pre-processing and supervised classification. Ground-truth information was utilized for validation of the result.

The classification analysis shows that built-up area had increased positively throughout the study period, while cultivated land decreased. Water bodies, bare land, forest cover, and grass land had also witnessed positive and negative changes. The NDVI and NDBI values also highlight negative changes in vegetation biomass and positive changes in built-up areas in Awka.

The study shows that remote sensing (RS) and geographic information systems (GIS) are effective tools for studying land use patterns. It suggests using the tools as a foundation for planning and decision-making. Hence, land use analysis should be observed and updated periodically

Keywords: Climate change, Cultivated land, Food insecurity, Forest cover, Land-use, SDGs.

INTRODUCTION

Anthropogenic processes and their driving forces have profoundly altered the world's ecosystems. As a result of these alterations, only a small portion of these landscapes still retain their original form (Chang *et al*., 2018; Esa *et al*., 2018). As man continues to exploit his environment, a situation is reached where its natural state is devastated (Singh *et al*., 2015; Bazai & Panezai, 2020). Teshome *et al.* (2022) assert that these devastations can be traced to demographic pressure, which persists as man explores his environment through deforestation, agriculture, and urbanization (Ariti *et al*., 2015; Msofe *et al*., 2019). These exploitations of natural resources have led to land-use change (hereafter LUC). According to Osman *et al*. (2023), understanding LUC is increasingly important for managing the available ecosystems and then keeping track of their changes through time at the local, regional, and global levels (Zenebe *et al*., 2018; Rigden & Li, 2017). LUCs are the results of historical processes as human activities, agricultural practices, technological developments, and societal growth has shaped the natural landscapes into their current configurations (Enoh *et al*., 2022). It is the alteration of resources, including water, soil, and vegetation, and the direct impartation of groundwater infiltration, run-off, and evapotranspiration (Chakilu & Moges, 2017; Hegazy & Kaloon, 2015; Sewnet, 2015). LUC are inherently linked to human existence and can be traced to natural and anthropogenic drivers. It is motivated by man's desire to acquire food, energy, and other resources in its environment (Saifullah *et al*., 2017; Yuan *et al*., 2015). The natural drivers of LUC are identified as flooding, fire, weather, erosion, desertification, drought, and volcanic eruptions. Anthropogenic drivers include population expansion and have been reported to impact resources such as forest cover (*FR*), cultivated land (*CL*), wetlands, and green spaces, resulting in losses (Zhou *et al.,* 2017; Yirsaw *et al*., 2017).

The UN's member states created the 2030 Agenda to address global concerns (UN 2015). The Agenda contains 17 sustainable development goals (SDGs), 169 globally recognized targets, and 232 indicators in light of the accomplishment of the Millennium Development Goals (MDGs) (Fu *et al*., 2017; UN, 2015). While the targets explain the objectives, the indicators serve as a gauge of their achievement. The SDGs are not isolated. They acknowledge that development is interrelated, meaning that decisions made in one location can affect others made in another location. Accordingly, if we halt deforestation and enhance the forest cover (SDG 15), food insecurity will be improved (SDG 2) and climate change will be mitigated (SDG 13). Hence, the SDGs is a universal roadmap for all countries to follow in order to attain a sustainable future by 2030. According to the World Bank, the SDGs are a call to action for all countries to raise their standard of living while eradicating hunger, poverty, and environmental degradation (United Nations and Nations, 2015). SDG-2 focuses on accomplishing "zero hunger". Its stated goals include eradicating hunger, improving nutrition, achieving food safety, and advancing sustainable agriculture. According to reports by the United Nations (UN, 2015), approximately 690 million people, which roughly represent 10 % of the world population, are undernourished. The first five SDG-2 targets (2.1–2.5) are directly linked to food safety and agricultural sustainability, while the latter three (2a–2c) pertain to markets intended to encourage agricultural investment and reduce market barriers, distortions, and volatility. SDG 13 urges us to mitigate the impact of climate change (Enoh *et al*., 2023). It addresses a range of issues related to climate change with five goals and eight indicators.

Conventional ground techniques have often been used to analyze the impact of LUC on *FR* and *CL*. These methods, which include field surveys, maps, and available records, are time-consuming, labor-intensive, vigorous, and infrequent (Ayele *et al*., 2018; Hc *et al*., 2020). With conventional methods, land use (hereafter LU) maps quickly become obsolete,

especially in terrains where information regarding LU changes rapidly (Dash *et al*., 2015). Remote sensing (RS) has been provided as an alternative method to traditional techniques. RS is more valuable and cost-effective for monitoring LU changes (Chew *et al*., 2016; Saleem *et al*. 2020; Malik *et al*., 2020). It can be integrated with Geographic Information System (GIS) techniques for rapid detection and mapping LUC (Pal & Ziaul, 2017; Kharazmi *et al*., 2018; Romaguera *et al*., 2018). Remotely sensed data covers a large geographic area and can provide vital information about the location, rate, nature, trend, and magnitude of LUC. Globally, RS and GIS have been established as important tools for analyzing LU spatial-temporal changes. Vegetation indices, an important aspect of RS, have been acknowledged and adopted for monitoring LU changes as well as extracting features of interest from satellite data. Among these indices are the normalized difference vegetation index (NDVI) (Congedo, 2020; Abebe *et al*., 2022), the normalized difference built-up index (NDBI) (Zha *et al*., 2003), the normalized difference snow index (NDSI) (Khan *et al*., 2005), and the normalized difference water index (NDWI) (Satir *et al*., 2016). The NDVI is the most popular method for identifying green vegetation. NDSI, NDWI, and NDBI have been identified as indices for extracting snow, water, and built-up areas, respectively. All over the world, the relevance of RS and GIS as tools to monitor urban LU spatial-temporal changes has been acknowledged. These tools were applied by researchers such as Appiah *et al*., 2021; Aderele *et al*., 2020; Hc *et al*., 2020; Satir *et al*., 2016; Fu *et al*., 2017; and Chew *et al*., 2016 to analyze the impact of LU changes on forest cover, cultivated land, urban green space, and wetland losses.

Awka has witnessed tremendous changes in its LU classes since its inception as the administrative capital of Anambra State, Nigeria. The city grew from an estimated population count of 104,682 in 1991 to 301,657 in 2006 (National Population Commission, 2013), and at a population growth rate of 2.2 %, Awka is simulated to reach a population count of approximately 507,600 by 2030 (24-year planning period). This statistic shows that the study area is expanding and quickly developing into a continually built-up area, which may transform into a large urbanized zone. Following the results, Awka's *FR* and *CL* may be exploited and converted into residential sites. This exploitation and degradation of the area's *FR* and *CL* have been found to be the major reasons for food insecurity and climate change in the zone. Research findings have shown that despite persistent LU changes in Awka, there are no up-to-date LU classification records, which are relevant for the achievement of a sustainable city. As a follow-up, this study intends to fill the identified gap. It involves analyzing the impact of LU changes on *FR* and *CL* in Awka from 2010 to 2020. It views built-up, as a key driver of these changes, which can result in climate change and food insecurity. This study also intends to serve as an improvement over many citations analyzed in LU studies, as it relates LUC dynamics to the UN's SDGs. In this study, Landsat 7 ETM+ and 8 OLI were the RS datasets adopted for the classification analysis, and the maximum likelihood post-classification method was utilized to identify the LUC dynamics. Other analyses identified in the study to analyze the LUC were net change, accuracy assessment, and transition analysis.

DESCRIPTION OF THE STUDY AREA

Awka is the administrative capital of Anambra, a state in Nigeria. The city is located between latitudes 6 °09'N and 6 °19'N and longitudes 7 °01'E and 7 °12'E. Awka is found between Onitsha and Enugu, two important cities in southeastern Nigeria. Some important towns that make up Awka and its environs are Nibo, Amawbia, Nise, Mgbaku, Umuawulu,

Isiagu, Ezinato, and sections of Okpuno, Amansea, Urum, and Nawgu (Fig. 1). The soils that characterize the study area are lateritic, with a red or brown color, and prone to flooding. The rivers that drain the area are Haba, Obizi, and Obibia in the south; Obizi Okpuno in the north; and the Mamu River in the east (Ezenwali *et al*., 2014). Awka's vegetation cover is predominantly deciduous trees. These trees include palm trees, raffia palms, iroko trees, oil bear trees, and gravelina trees. Awka has a tropical wet and dry climate with a distinct seasonal cycle. Its wet season runs from April to September, with frequent thunderstorms and lightning. Awka's dry season lasts for six months. It begins in October and ends in March with harmattan weather, which is dry, dusty, and reduces visibility (Nzoiwu *et al*., 2016). Annually, Awka receives approximately 1,600 mm of rain. Its temperature is between 27 °C-30 °C during the months of June and December but rises to 32 °C-34 °C during the latter months of the dry season (Ezenwali *et al*., 2014). Awka is predominantly inhabited by the Igbo people, who are known for their low income, unemployment, and restricted access to basic healthcare. These issues are frequently connected to substandard housing and inadequate education.

Fig. 1: Map of (a) Africa, (b) Nigeria, (c) Awka and its environs

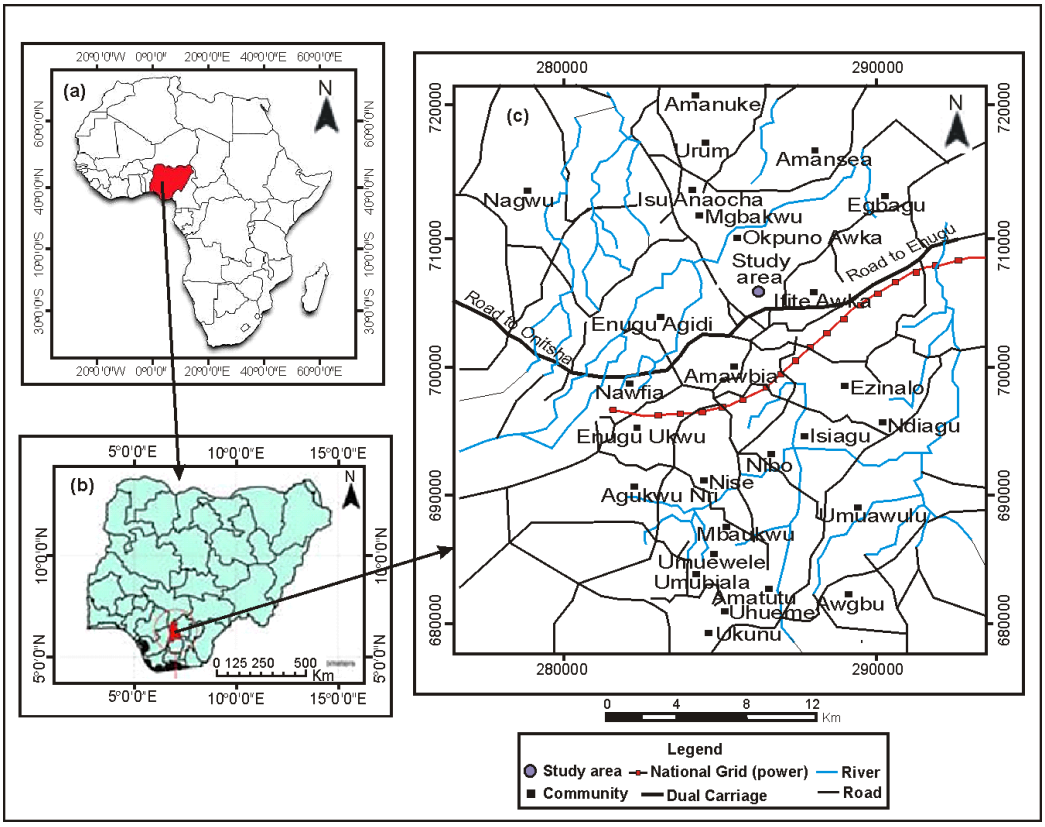

MATERIALS AND METHODS

Data acquisition and their sources

In this study, three cloud-free remotely sensed data sets, namely Landsat 7 ETM+ 2010 and 8 OLI (2015 and 2020), were used to examine the LU change dynamics. The data were acquired from the United States Geological Survey portal (http://earthexplorer.usgs.gov/) with path 188 and row (55, and 56) and then projected to a 32 N UTM map zone using a WGS 84 datum. Ground control points (GCPs) were used to georectify the satellite data collected in January (the same months) with the aim of minimizing classification error and preventing seasonal changes (Verpoorter *et al*., 2012). Table 1 depicts the parameters of the study's Landsat sensor. Fig. 2 is the study's methodological flow diagram. It shows auxiliary, Landsat ETM+, OLI, and ground truth as datasets acquired for this study. The Landsat data (ETM+ and OLI) were pre-processed and classified using the supervised classification approach (maximum likelihood classifier) to produce the LU maps of the study periods (2010, 2015, and 2020). Accuracy assessment was observed to ascertain the accuracy of the classification process. Change analysis and change maps were also produced using the land change modeler (LCM) tool embedded in the IDRISI Selva program.

Table 1: Parameter of study's Landsat sensor

Satellite Name	WRS Path/Row	Sensor Type	Cloud Cover (%)	Date of Acquisition	UTM Zone	Spatial Resolution (Meters)
Landsat 7	188/055, 188/056	ETM+	<10%	10/01/2010	32 N	30x30
Landsat 8	188/055, 188/056	OLI/TIRS	<10%	12/01/2015	32 N	30x30
Landsat 8	188/055, 188/056	OLI/TIRS	<10%	11/01/2020	32 N	30x30

Fig. 2: The study's methodology flow diagram

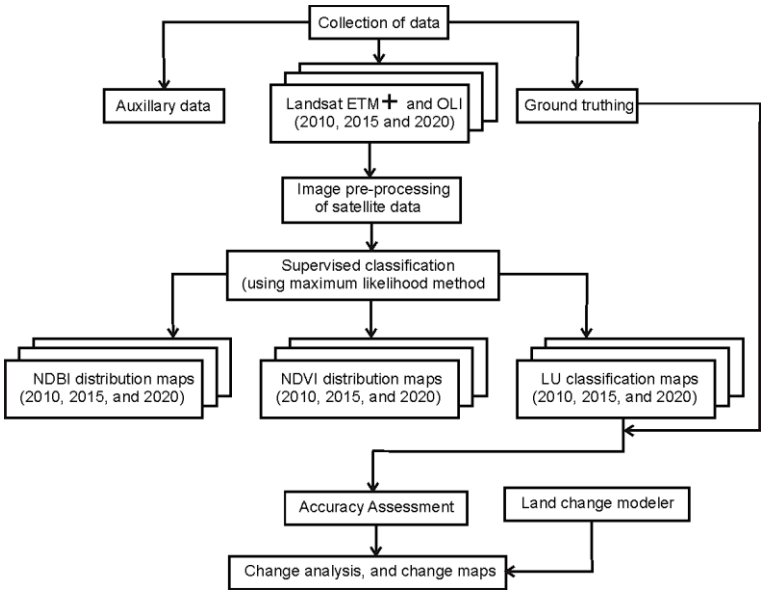

Preprocessing

Preprocessing is crucial in change detection analysis, as imperfections attributed to image sensors, atmospheric conditions, and the curvature of the Earth, if not corrected, might lead to incorrect results (Parsa *et al*., 2016). Preprocessing enhances image quality by reducing or eliminating radiometric and geometric errors (Islam *et al*., 2018; Enoh *et al*., 2022). In our study, preprocessing was carried out with Erdas Imagine (ver. 2015) and the ArcGIS 10.5 program. Here, gap filling, subsetting, and enhancement were performed on the Landsat satellite data. Landsat 7 ETM+ data acquired after May 31, 2003, often show traces of a zig-zag pattern over the satellite ground route (Fig. 3a). This error came into existence as a result of a failure in the ETM+ sensor's scan line corrector (SLC). The failure resulted in gap lines and a loss of approximately 22 % of the scene (Langford, 2015). For our study, we use the Landsat toolbox embedded in the ArcGIS program to pre-process the zig-zag pattern displayed in the Landsat 7 ETM+ (2010) data (Fig. 3b). To highlight the visual perception of the study's remotely sensed data, a false color composite (FCC) was created by combining spectral image bands in the RGB format (4, 3, and 2) for ETM+ data (Fig. 4a) and (5, 4, and 3) for OLI/TIRS (Fig. 4b and 4c). The image was enhanced with the histogram equalization tool and sub-set with the shape file of the study area, in order to create the area of interest (AOI). The enhanced images were co-registered with the Universal Transverse Mercator (UTM) zone 32N coordinate system on the 1984 World Geodetic System (WGS) ellipsoid.

Fig. 3: The study's Landsat 7 ETM+ (2010) sensor before and after the zig-zag pattern remova

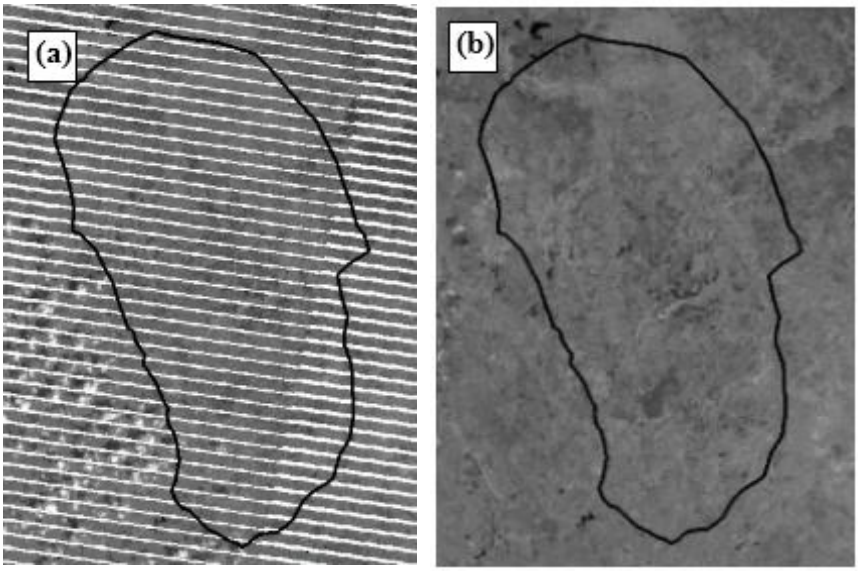

ETM+ sensor (a) before zig-zag pattern removal (b) after zig-zag pattern removal

Fig. 4: False color composite (FCC) of Landsat sensors for 2010, 2015, and 2020

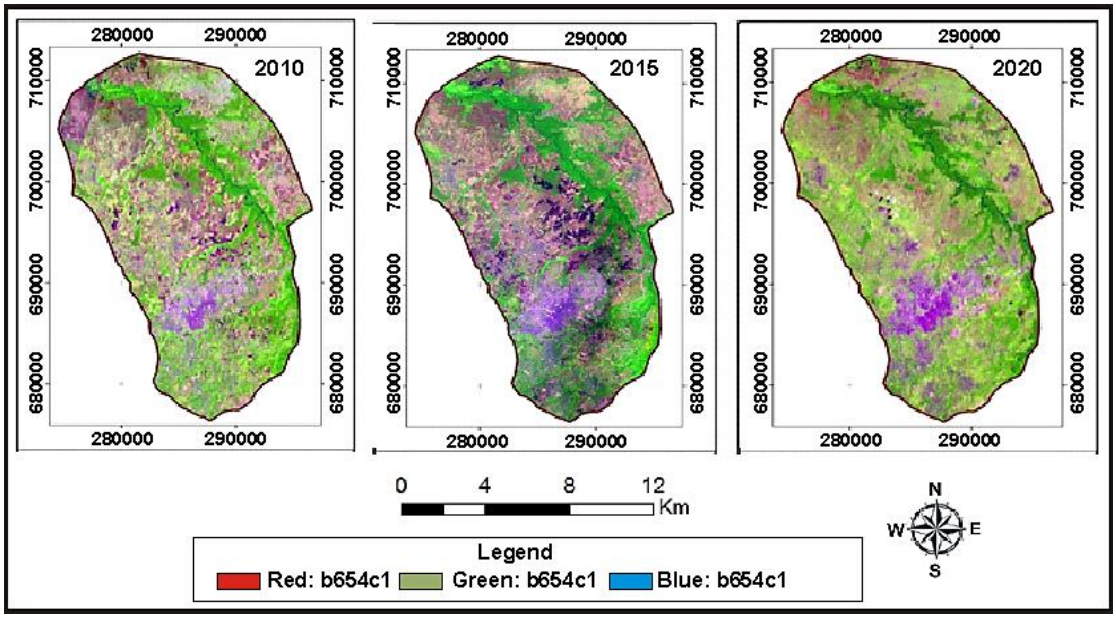

Image Supervised Classification

Supervised image classification is an important technique in remote sensing (Wang *et al*., 2015). It aids in the detection, identification, and classification of image features by highlighting the LU classes they depict on the earth's surface (Al-Sharif & Pradhan, 2013). In our study, the maximum likelihood classifier (MLC) was adopted as a technique for classification due to its ease of training and availability (Tariq *et al*., 2022; Zainab *et al*., 2021). This approach to classification was based on our expertise, visual interpretation, and understanding of the study area's physiography (Ratnaparkhi *et al*., 2016; Zubair & Javed, 2018). Image clusters are defined as LU classes in the supervised classification process, and each class frequently occupies a feature space. It involves delineating training sites, which we defined according to Anderson *et al*.'s (1976) classification scheme. The training involved grouping similar pixels into a category based on their spectral pattern. Table 2 defines the classification scheme adopted for this study. In our study, ERDAS Imagine 2014 and ArcGIS 10.5 were the software adopted for the classification process.

Table 2: The study's classification scheme (after Anderson *et al*., 1976)

LU classes	Description
Built up (*BU*)	These include residential, commercial, and industrial sites.
Forest (*FR*)	These covers areas of dense and coniferous trees.
Water body (*WB*)	This includes rivers, lakes, streams, gravel, canals, and reservoirs.
Bare land (*BL*)	These are areas of barren land; boulders; stock quarries; dump sites; exposed soil; and active excavation.
Cultivated land (*CL*)	These are areas of permanent and annual crops and for irrigation sites.
Grass land (*GL*)	These are areas covered with grass, meant for grazing sites.

Accuracy Assessment

Accuracy assessment is the final stage of the image classification process. It utilizes a stratified random approach to represent different LU classes. Based on the ground truth information and visual interpretation, an error matrix was used to compare the reference data with the classification results as a square array that equates the number of LU classes being assessed to the number of classes in rows and columns (Disperati &Virdis, 2015). The correctly classified entries are displayed as diagonal, while non-diagonal entries are omissions (non-diagonal column entries) or commissions (non-diagonal row entries). Other accuracy measures, namely overall accuracy (OA), producer accuracy (PA), and user accuracy (UA), are also computed (Coppin *et al*., 2004; Boschetti *et al*., 2004). PA is computed as the correctly categorized pixels divided by the total reference pixels for the selected class (Bradley, 2009; Mohammady *et al*., 2015). UA is calculated by dividing the correctly classified pixels by the total classified pixels, and OA is the total number of correctly categorized pixels divided by the total number of pixels for all classes (Congalton & Green, 2019; Liu *et al*., 2007). The Kappa test (*K*) compares predetermined producer ratings with ratings supplied by users. *K* is rated strong to perfect agreement if its value is greater than 0.8. It is moderate if its agreement is between 0.6–0.8, and good agreement if it is between 0.4–0.6. (Fardaus *et al*., 2014; Ziyad & Prakash, 2020). *K* can be computed with equation I:

$$K = \frac{N\sum_{i=1}^{n} X_{ii} - \sum_{i=1}^{n} X_{i+}X_{+i}}{N^2 - \sum_{i=1}^{n} X_{i+}X_{+i}} \qquad (1)$$

Where *N* is the total number of observations; *K* is the Kappa coefficient; r is the matrix's number of rows; *X*ii is the total observations in row *i;* and in column *I*, *X*i+ is row *i*'s marginal total and *X* + *i*'s marginal total.

LU change detection

LU Post-Classification

In our study, the Post-Classification (PC) method was used to analyze the LU changes (Firdaus *et al*., 2014; Ziyad & Prakash, 2020). Here, PC was performed with ArcGIS 10.5 and the Idrisi Selva program to generate a cross-tabulation of two thematic maps by overlay operation. During the operation, cross-tabulation produces pixel agreement and disagreement, which are determined by the error matrix table. In the table, the reference data are represented in rows, while the classified data are in columns (Teferi *et al*., 2013). Thematic maps generated for 2010, 2015, and 2020 are used for the 2010–2015, 2015–2020, and 2010–2020 relationships in order to analyze the net change (gain or loss), change maps, change matrix, and transition probabilities for the respective LU study classes.

Net Change (Gain and Loss Analysis)

Net change analysis is computed as differences between gains and losses for each LU class (Pontius *et al*., 2004; Teferi *et al*., 2013). Gains are the amount of LU class *i* that is added from time 1 to time 2, while losses are the lost LU class *j* during the classification process between time 1 and time 2. In our study, gain and loss dynamics were determined with cross-tabulation analysis.

LU change analysis

Change analysis is the process of computing the differences between the timing of an object (Singh, 2017; Rawat & Kumar, 2015). In remote sensing, overlay operation is a technique that relates to change analysis. It involves observing pixel-by-pixel comparisons in order to determine the pixels that changed during the classification analysis. (Abebe *et al*., 2019; Abraham *et al*., 2016; Mozumder & Tripathi, 2014). By overlaying, a new image is formed to highlight changes that took place during the classification process. Change trend (*CT*), and change percentage (*CP*) are operations linked with change analysis. *CT* is a technique that is often used to measure the magnitude of change between two LU classes. It can be negative (-) or positive (+). It is negative if the LU classes are decreasing and positive if they are increasing in size (Teferi *et al*., 2013). CP is computed using the values of *CT* according to equations 2, and 3.

$$\text{Change trend } (CT) = A_2 - A_1 \quad (2)$$

$$\text{Change percentage } (CP) = \left(\frac{A_2 - A_1}{A_1} * 100 \right) \quad (3)$$

Where n is the time in seconds between the areas A_1 and A_2 (in years). A_2 and A_1 are expressed in km^2.

Estimation of the Normalized Difference Vegetation Index (NDVI)

NDVI is one of the most important indices that can be used to study the health status of green vegetation. It is estimated with remote sensing data based on the spectral characteristics of vegetation. NDVI absorbs visible light from vegetation and photosynthetic energy and reflects near-infrared (NIR) radiation (Forkel *et al*., 2013; Kidane *et al.,* 2019; Yuan *et al*., 2015). In our study, NDVI was computed from ETM+ 2000 and OLI (2015, 2020). It is an indicator created to distinguish green vegetation from other surfaces based on the vegetation reflectance characteristics of the area (Naz & Rasheed, 2017; Zoungrana *et al*., 2018). NDVI measurements range from -1 to +1 (Khan *et al*., 2020; Rizvi *et al*., 2020). NDVI values higher than zero depict the presence of green vegetation. The higher the NDVI value, the higher the likelihood that an area on the ground is densely covered in green vegetation. Negative values of NDVI depict the absence of green vegetation cover and areas covered with water bodies. In this research, NDVI was computed using equation 5, with its final values grouped as low and high NDVI (Usman *et al*., 2013; Mohammed *et al*., 2019).

$$\text{Normalized Difference Vegetation Index } (NDVI) = \left(\frac{\text{NIR}_{\text{(Band 4,5)}} - \text{Red}_{\text{(Band 3,4)}}}{\text{NIR}_{\text{(Band 4,5)}} + \text{Red}_{\text{(Band 3,4)}}} \right) \quad (4)$$

Where $\text{NIR}_{\text{(Band 4)}}$ for Landsat 4-5 TM is 0.76-0.90 µm, and $\text{NIR}_{\text{(Band 5)}}$ for Landsat 8 OLI is 0.85-0.88 µm. For Landsat 4-5 TM and Landsat 7 ETM+, $\text{RED}_{\text{(Band 3)}}$ is 0.63-0.69 µm, and $\text{NIR}_{\text{(Band 4)}}$ is 0.64-0.67 m for Landsat 8 OLI.

Estimation of the Normalized Difference Built-up Index (NDBI)

The normalized difference built-up index (NDBI) is another important index that is often used to extract information about the extent of built-up regions from remotely sensed data (Bhatti & Tripathi, 2014). As opposed to other LU areas, built-up areas reflect more light at

the MIR wavelength of 1.55–1.75 μm and the NIR wavelength of 0.76-0.90 μm. Built-up values range from -1 to +1. Higher NDBI values indicate a high-density built-up area, and low NDBI values depict a low-density built-up area distribution. NDBI can be computed using equation 6 (Zha *et al*., 2003).

$$\text{Normalized Difference Built-up Index } (NDBI) = \left(\frac{\text{MIR}_{\text{(Band 5,6)}} - \text{NIR}_{\text{(Band 4,5)}}}{\text{MIR}_{\text{(Band 5,6)}} + \text{NIR}_{\text{(Band 4,5)}}} \right) \quad (5)$$

Where $\text{MIR}_{\text{(Band 5)}}$ for Landsat 4-5 TM and Landsat 7 ETM+ is 1.55-1.75 μm, and $\text{MIR}_{\text{(Band 6)}}$ for Landsat 8 OLI is 1.57-1.65 μm. For Landsat 4-5 TM and Landsat 7 ETM+, $\text{RED}_{\text{(Band 4)}}$ is 0.76-0.90 μm, and $\text{NIR}_{\text{(Band 5)}}$ is 0.85-0.88 m for Landsat 8 OLI.

RESULTS AND INTERPRETATION

Table 3(a) depicts the overall area and percentage of LU class categories and their associated changes from 2010 to 2020. According to the study, *BU* and *GL* class areas had respectively increased from 98.56 km^2 (18.99 %) and 104.30 km^2 (20.10 %) in 2010 to 113.35 km^2 (21.84 %) and 118.11 km^2 (22.76 %) in 2015 and to 145.41 km^2 (28.02 %) and 185.48 km^2 (35.74 %) in 2020. In contract, *CL* decreased from 69.40 km^2 (13.37 %) in 2010, to 20.92 km^2 (4.03 %) in 2015, and to 7.44 km^2 (1.43 %) in 2020. *FR*, *WB*, and *BL* classes had also changed. *FR*, *WB*, and *BL* changed from 139.92 km^2 (26.96 %), 7.05 km^2 (1.36 %), and 99.79 km^2 (19.23 %) in 2010 to 116.41 km^2 (22.43 %), 32.34 km^2 (6.23 %), and 117.89 km^2 (22.71 %) in 2015, and to 126.51 km^2 (24.38 %), 8.56 km^2 (1.65 %), and 45.62 km^2 (8.79 %) in 2020.

Table 3: The study's classification analysis in area and in percentage

(a) LU Classes	Area in square kilometer			Area in percentage		
	2010	**2015**	**2020**	**2010**	**2015**	**2020**
Built up (*BU*)	98.555	113.352	145.407	18.989	21.840	28.016
Forest (*FR*)	139.922	116.410	126.509	26.959	22.429	24.375
Water body (*WB*)	7.052	32.335	8.564	1.359	6.230	1.650
Bare land (*BL*)	99.788	117.887	45.616	19.226	22.714	8.789
Cultivated land (*CL*)	69.403	20.917	7.441	13.372	4.030	1.434
Grass land (*GL*)	104.295	118.114	185.478	20.095	22.757	35.737
Total	**519.015**	**519.015**	**519.015**	**100**	**100**	**100**
(b) LU Classes	**Change trend (*CT*) (in Km^2)**			**Change percentage (*CP*) (in %)**		
	(2010–2015)	**(2015–2020)**	**(2010–2020)**	**(2010–2015)**	**(2015–2020)**	**(2010–2020)**
Built up (*BU*)	14.797	32.055	46.852	15.01	28.28	47.54
Forest (*FR*)	-23.512	10.099	-13.413	-16.80	8.68	-9.59
Water body (*WB*)	25.283	-23.771	1.512	358.52	-73.51	21.44
Bare land (*BL*)	18.099	-72.271	-54.172	18.14	-61.31	-54.29
Cultivated land (*CL*)	-48.486	-13.476	-61.962	-69.86	-64.43	-89.28
Grass land (*GL*)	13.819	67.364	81.183	13.25	57.03	77.84

Table 3(b) highlights the change trend (*CT*), change percentage (*CP*), and annual rate of change (*R*) of the study classes. During the first phase (2010–2015), second phase (2015–2020), and third phase (2010–2020) of the study, *BL* and *GL* classes had changed positively

by 14.80 km^2 and 13.82 km^2; by 32.06 km^2 and 67.36 km^2; and by 46.85 km^2 and 81.18 km^2. The positive change in the *BL* classes may be a result of infrastructural development, population growth, and immigration. Similarly, the positive change in the *GL* may be traced to low grazing, low encroachment, and a favorable climate. *CL* had changed negatively by 48.49 km^2 during the first period, by 13.48 km^2 during the second period, and by 61.96 km^2 during the third period. The negative change in *CL* may be linked to the neglect of farming activities as well as the conversion of farmlands into *BA* areas. *FR*, *WB*, and *BL* had changed positively and negatively during the first, second, and third phases. The areas changed by -23.512 km^2, 25.28 km^2, and 18.10 km^2 during the 2010–2015 phase, 10.10 km^2, -23.77 km^2, and -72.27 km^2 during the 2015–2020 phase, and -13.41 km^2, 1.51 km^2, and -54.17 km^2 during the 2010–2020 phase.

Fig. 5: The study's LU supervised classification maps of Awka during 2010, 2015, and 2020 years

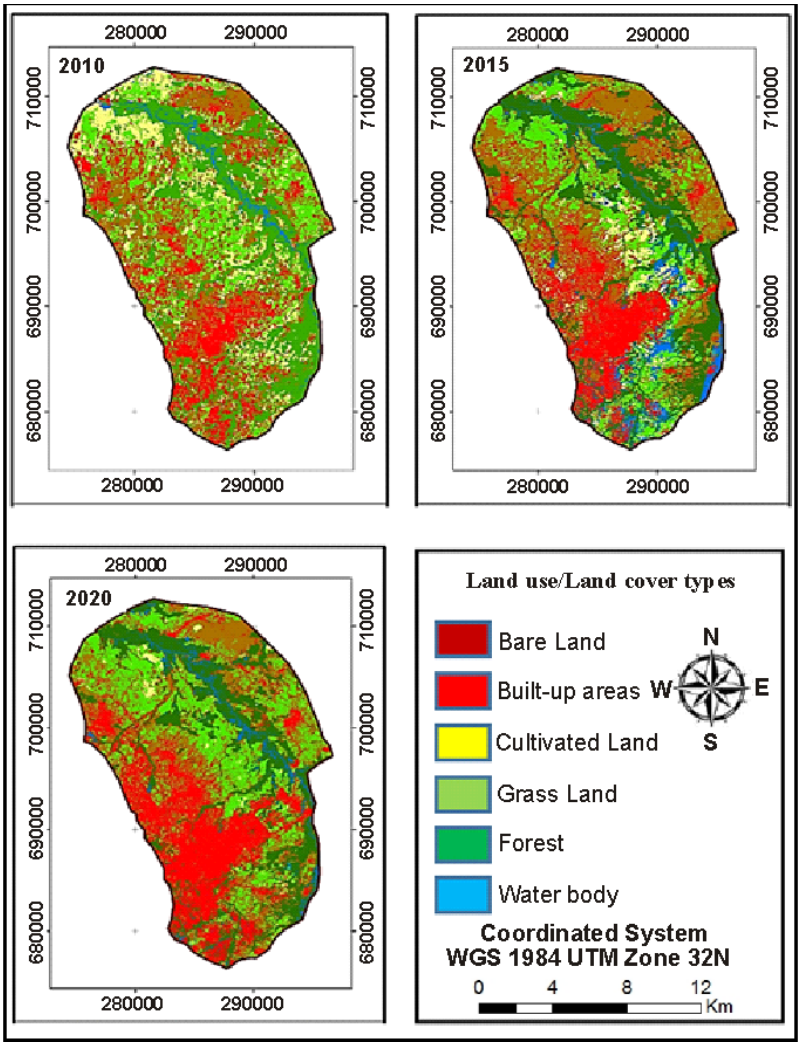

The positive change in the FR cover may be a result of forest conservation practices, including tree regeneration practices. The negative change may be traced to deforestation and urbanization. The changes in WB may be due to sand deposition, land reclamation, and other developmental activities that exist along the coast. The changes in bare land may be linked to overgrazing, indiscriminate bush burning, and deforestation. Fig. 6 is a chart that depicts the study's classification analysis and change trend (*CT*).

Fig. 5 depicts the final supervised LU classification maps during the 2010, 2015, and 2020 study years. The maps are based on Landsat 7 ETM+ and 8 OLI data, with red pixels depicting built-up areas and brown, yellow, blue, light, and dark green pixels highlighting bare land, cultivated land, water bodies, grassland, and forest, respectively.

Change Detection analysis

LU Gains and Losses analysis

Table 4 illustrates the respective net changes (gains and losses) of the study's LU classes from 2010 to 2020. From the analysis, we see that during the first period (2010–2015), second period (2015–2020), and third period (2010–2020), cultivated land lost 500 km^2, 170 km^2, and 800 km^2 of their previously existing area to other LU classes, while also gaining 180 km^2, 90 km^2, and 20 km^2. Cultivated land may have lost its area because a greater part of it may have been converted to built-up areas. Similarly, forest cover suffers losses and also gains from other LU classes during the first, second, and third periods. *FR* lost 900 km^2, 710 km^2, and 550 km^2 during the first, second, and third periods, while also gaining 610 km^2, 680 km^2, and 330 km^2. The negative changes in the study's *FR* may be linked to deforestation, urban development, and logging activities. Other LU classes also recorded losses and gains during the study periods. Fig. 6 is a chart that depicts the losses, gains, and net changes of the study's LU classes.

Table 4: Net change (Gains and losses) analysis

LU Classes	2010-2015 (Period 1) (in km^2)			2015-2020 (Period 2) (in km^2)			2010-2020 (Period 3) (in km^2)		
	Losses	Gains	Net change	Losses	Gains	Net change	Losses	Gains	Net change
Built up (*BU*)	-500	750	250	-610	580	-30	-530	650	120
Forest (*FR*)	-900	610	-290	-710	680	-30	-550	330	-220
Water body (*WB*)	-48	200	152	-190	110	-80	-20	100	80
Bare land (*BL*)	-680	980	300	-900	600	-300	-720	820	100
Cultivated land (*CL*)	-500	180	-320	-170	90	-80	-800	20	-780
Grass land (*GL*)	-700	720	20	-570	1150	580	-480	1050	570

Fig. 6: Charts depicting gains and losses (in km^2) for the study's LU classes

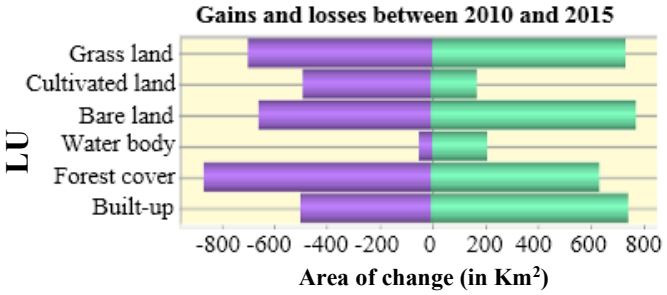

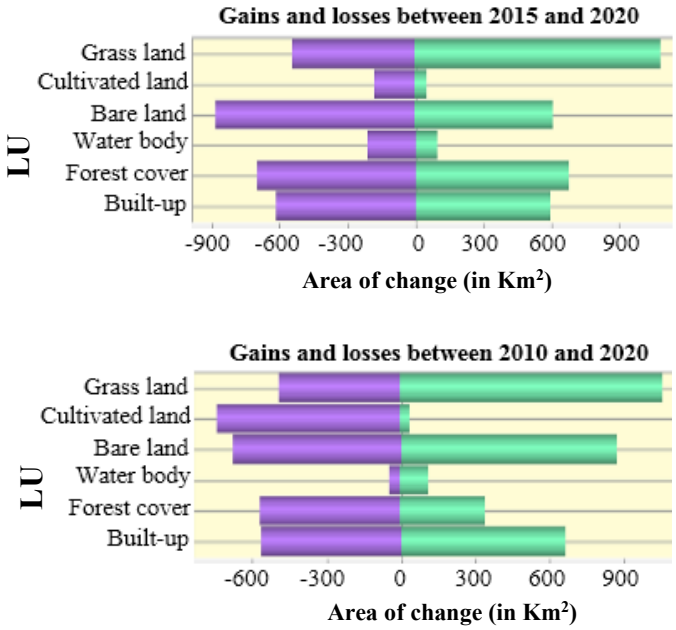

Fig. 7 shows maps that show the study's net change (gain and loss) analysis during 2010 and 2020, based on Landsat 7 (ETM+) and 8 (OLI) satellite data. The maps were prepared with a focus on built-up areas, forest areas, water bodies, bare land, cultivated land, and grass land as the respective LU types.

Contribution to net change experienced by the study classes

Fig. 8 shows charts that identify the major contributors to LUC in the study classes. The chart was prepared with the Land Change Modeler (LCM) tool embedded in the IDRISI GIS program. From the chart, we see that in Fig. 8(a)–(b), cultivated land is the major contributor to build-up and grassland areas, followed by bare land and forest cover. This shows that built-up area is one of the key drivers of cultivated land loss in the study area. In Fig. 8 (c), cultivated land is the only LU class that contributes to forest cover. Cultivated land contributed to BU, GL, and FC as part of its area may have been converted to BU sites, grassland, or used up for developmental activities. Fig. 8 (d)–(e) shows that forest cover was the largest contributor to water bodies and bare land, followed by cultivated land. Forest cover had contributed to WB and BL, as part of its area may have been submerged, exploited, or degraded for developmental activities. In Fig. 8(f), none of the study's LU classes contributed to cultivated land. This implies that farming activities are depreciating in the study area as cultivated land is being used up by other LU classes.

Fig. 7: Net changes in the study's LU classes

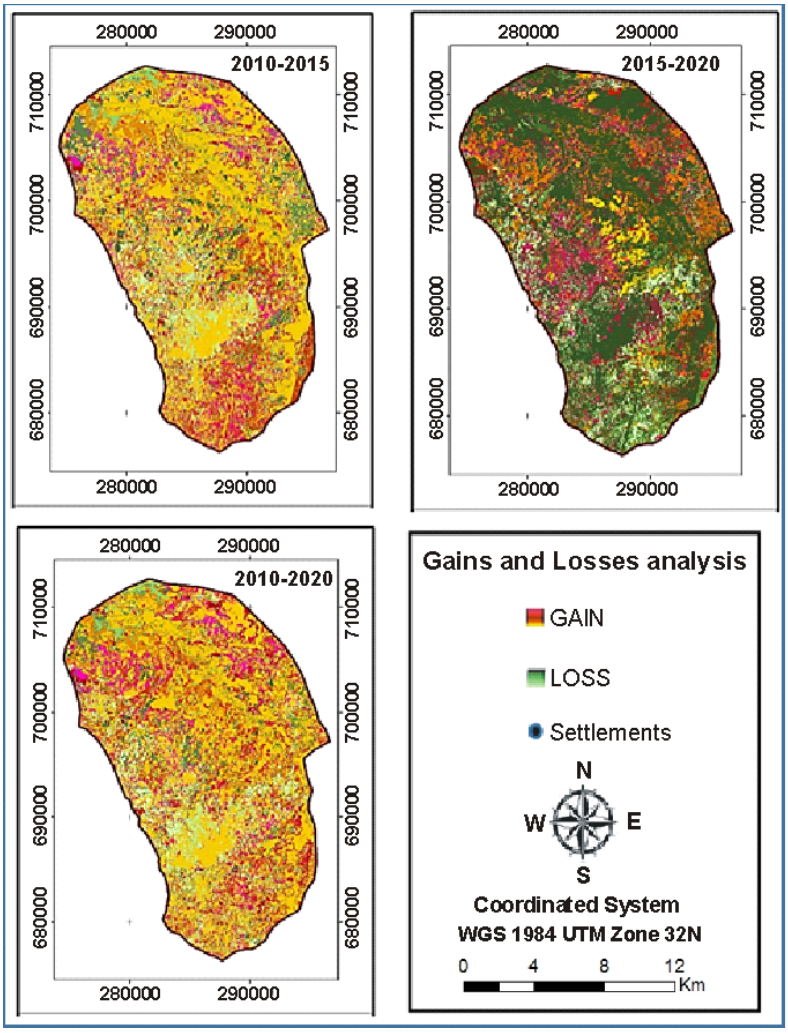

Fig. 8: Contributions to Net Change

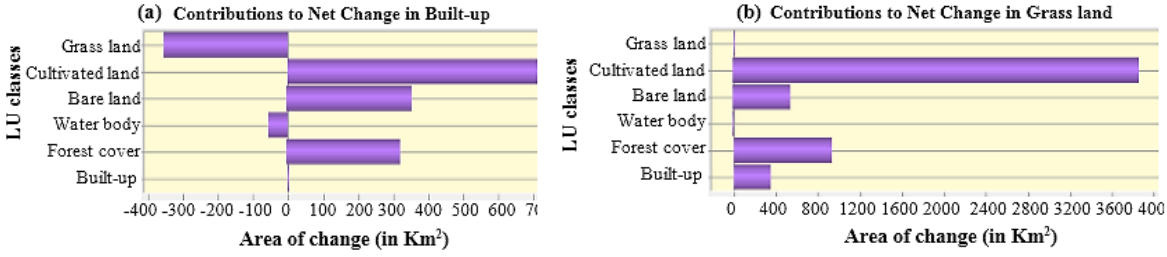

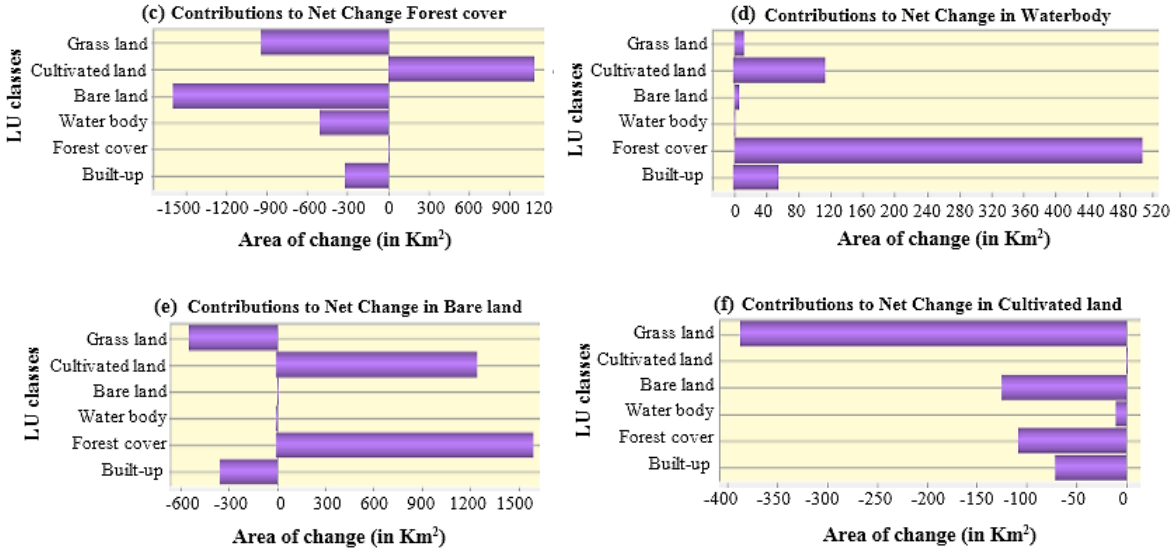

Transition Matrix

Table 5 is a transition matrix table that shows the study's transition analysis between 2010–2015, 2015–2020, and 2010–2020. The analysis reveals that during the 2010–2015 period, built-up areas, forest cover, and grassland were more stable, while cultivable land and grassland were transition classes. The transitions from cultivated land to grassland and from grassland to bare land were 6.2 % and 5.8 %, respectively. Water bodies had the least transition during this period. Between 2010 and 2020, built-up areas, forest cover, and grassland were constant, while the transition from cultivated land to grassland areas was the most significant. Fig. 11 is a map that shows the transition classes during the 2010–2020 period.

Table 5: The study's LU transition analysis (2010-2020)

	LU classes	**2020**					
		Built-up (*BU*)	Forest cover (*FR*)	Water body (*WB*)	Bare land (*BL*)	Cultivated land (*CL*)	Grass land (*GL*)
2010	Built up (*BU*)	41.7861	0.1035	0.0675	12.1752	0.6570	6.0858
	Forest (*FR*)	0.0864	51.9309	2.2563	0.9594	22.7331	5.1219
	Water body (*WB*)	0.0135	6.7617	6.9120	0.4212	3.1833	0.5337
	Bare land (*BL*)	13.4262	0.1521	0.3807	78.5700	4.5180	39.6171
	Cultivated land (*CL*)	0.5265	3.9816	0.5112	2.5092	34.6392	14.4270
	Grass land (*GL*)	17.2287	0.1719	0.0387	50.8779	14.0751	81.5553

Fig. 9: The study's LU transition map (2010-2020)

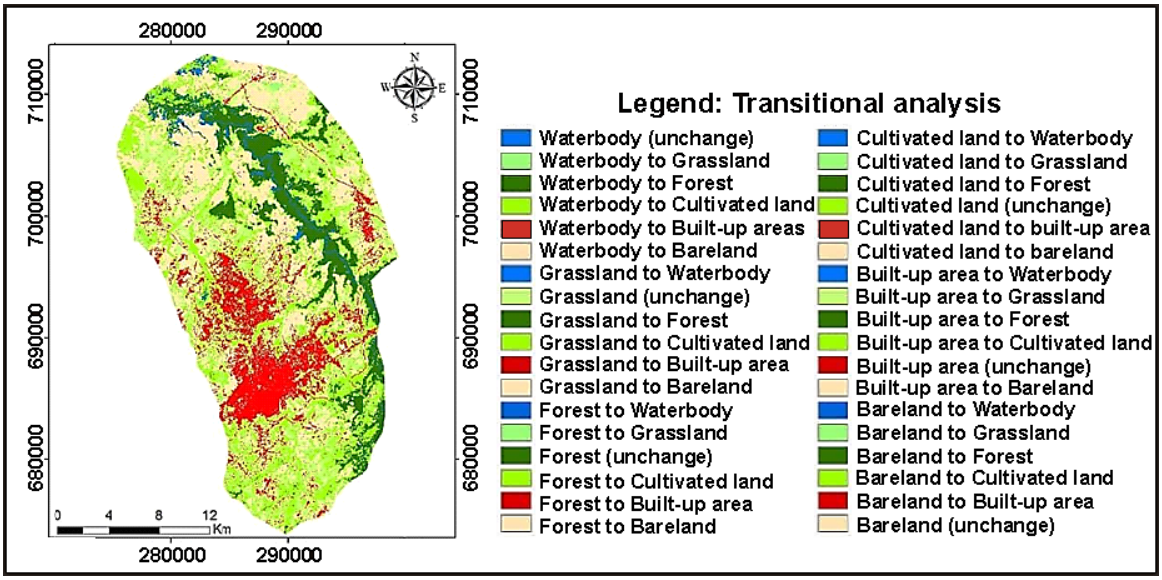

Normalized Difference Vegetation Index (NDVI) and Normalized Difference Built-up Index (NDBI) changes

Fig. 10 and 11 show the study area's NDVI and NDBI maps, which are quantified in Table 6. From our computation, we see that in 2010, the NDVI values ranged from 0.019 to 0.728. In 2015, the NDVI values changed to 0.021 (the minimum value) and 0.579 (the maximum value). In 2020, the minimum and maximum values were 0.038 and 0.537, respectively. The computation results show that the NDVI values are decreasing. This demonstrates the degradation of the area's vegetative biomass during the study period. The NDBI computation shows that the study's maximum NDBI values increased from 0.328 in 2010 to 0.530 in 2015 and to 0.549 in 2020. The Increase in NDBI values implies an increase in the study's built-up area. The decrease in the study's NDVI value and increase in its NDBI show that built-up areas are the major drivers of forest and cultivated land loss in Awka.

Table 6: Computation of NDVI and NDBI

Indices	2010		2015		2020	
	High	Low	High	Low	High	Low
NDVI	0.727965	0.0191564	0.579079	0.021	0.537054	0.0380106
NDBI	0.328131	-1.26044	0.530131	-0.345601	0.64893	-0.343272

Fig. 10: NDVI maps of Awka during 2010, 2015, and 2020 study years

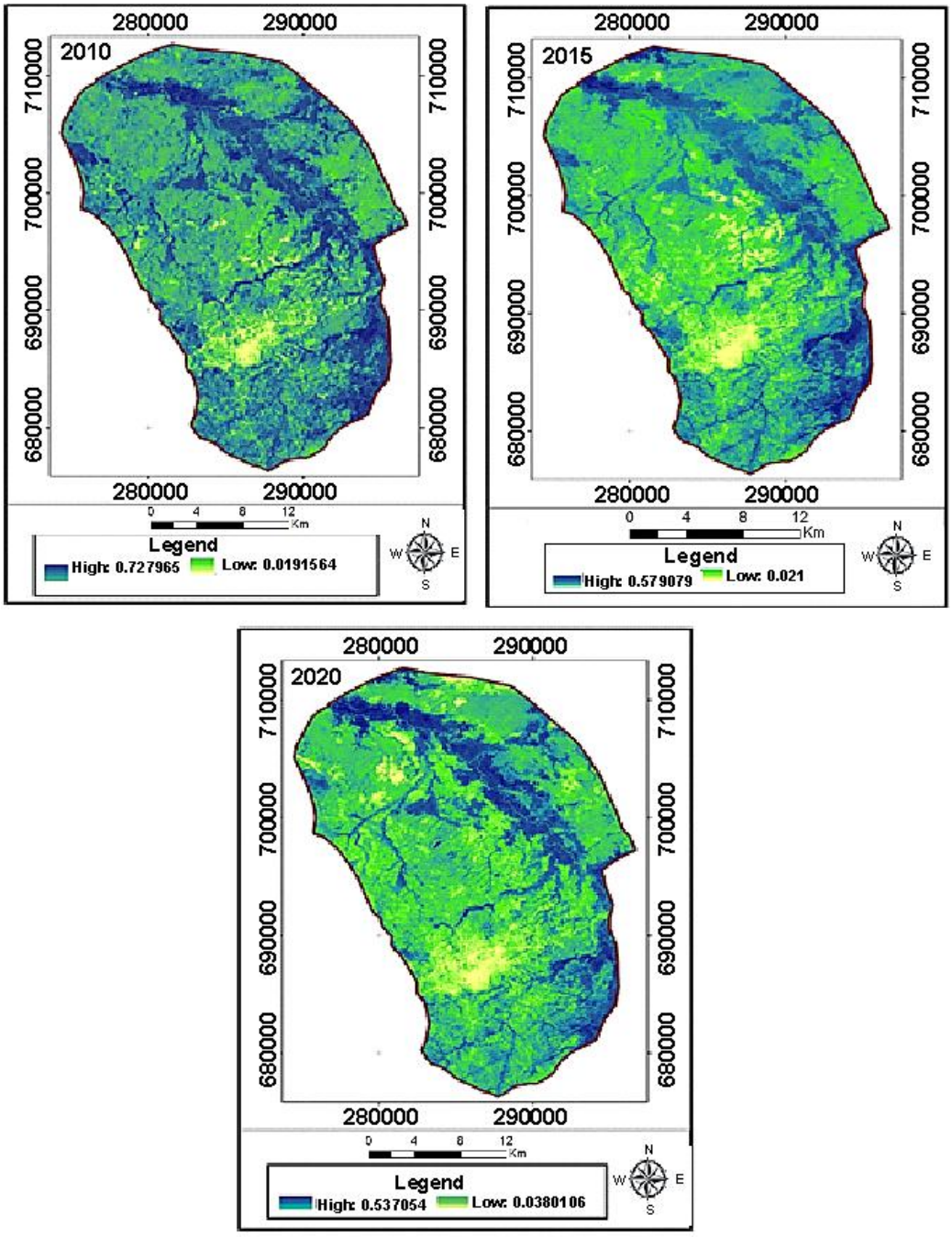

Fig. 11: NDBI maps of Awka during 2010, 2015, and 2020 study years

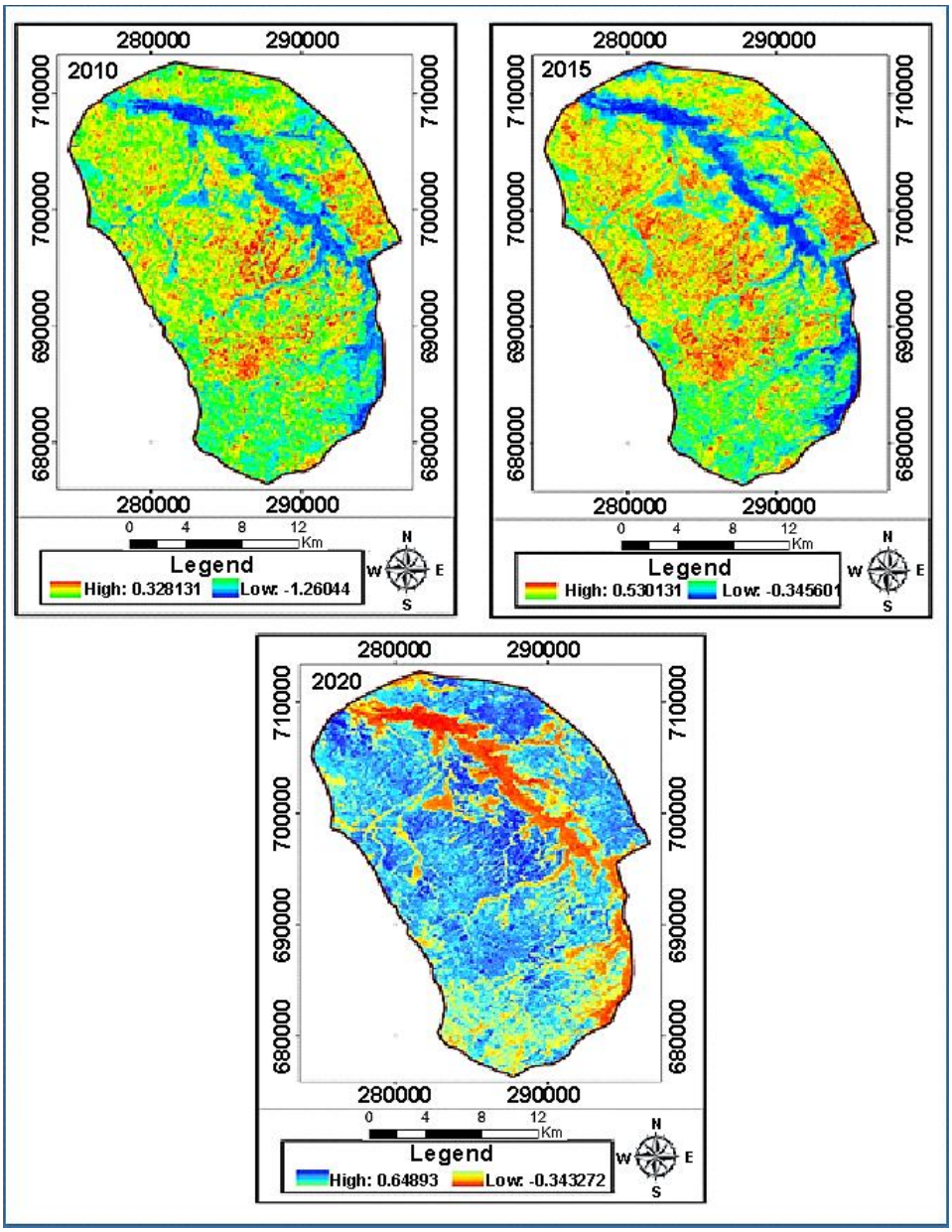

Accuracy Assessment

Table 7 is an error matrix table analyzed for the study. The accuracy evaluation was based on the creation of this table. It shows the overall accuracy and kappa statistics as 91.0 % and 0.86 in 2010; 85.0 % and 0.78 in 2015; and 83.0 % and 0.75 in 2020. Thus, the classification results are reliable, as the overall accuracy is high. The kappa coefficient is also acceptable.

Table 7: Error Matrix Table (2010-2020)

Error Matrix Table (2010)					
Class Name (2010)	Reference Totals	Classified Totals	Number Correct	Producers Accuracy	Users Accuracy
Bare land	7	7	5	71.43%	71.43%
Cultivated area	11	9	8	72.73%	88.89%
Forest cover	51	54	51	100.00%	94.44%
Built up	18	19	17	94.44%	89.47%
Grass land	12	10	9	75.00%	90.00%
Water body	1	1	1	100.00%	100.00%
Total	**100**	**100**	**91**		
Overall Classification Accuracy = 91.00%					
Overall Kappa statistics = 0.8644					
Error Matrix Table (2015)					
Class Name (2015)	Reference Totals	Classified Totals Number Correct		Producers Accuracy	Users Accuracy
Bare land	6	7	4	66.67%	57.14%
Cultivated area	14	9	8	57.14%	88.89%
Forest cover	50	54	48	96.00%	88.89%
Built up	17	19	16	94.12%	84.21%
Grass land	12	10	8	66.67%	80.00%
Water body	1	1	1	100.00%	100.00%
Bare land	6	7	4	66.67%	57.14%
Total	**100**	**100**	**85**		
Overall Classification Accuracy = 85.00%					
Overall Kappa statistics = 0.7757					
Error Matrix Table (2020)					
Class Name (2020)	Reference Totals	Classified Totals	Number Correct	Producers Accuracy	Users Accuracy
Bare land	9	7	6	66.67%	85.71%
Cultivated area	12	9	7	58.33%	77.78%
Forest cover	48	54	46	95.83%	85.19%
Built up	16	19	15	93.75%	78.95%
Grass land	12	10	8	66.67%	80.00%
Water body	3	1	1	33.33%	100.00%
Total	**100**	**100**	**83**		
Overall Classification Accuracy = 83.00%					
Overall Kappa statistics = 0.7504					

DISCUSSION

This study focuses on the use of RS and GIS as tools to analyze the impact of *LU* changes on forest cover and cultivated land in Awka. The UN outlines 8 targets and 13 indicators for achieving SDG 2. It also highlights 5 targets and 8 indicators for attaining SDG 13. The targets emphasize the goals, while the indicators are metrics that countries aim to comprehend. Tables 8(a)-(b) review and relate the study's findings to the selected SDG 2 and 13 targets and indicators.

Table 3 in Section 4 provides an overview of the findings of the LU changes in Awka. According to our research, the *BU* area increased from 98.56 km^2 (18.99 %) in 2010 to 113.35 km^2 (21.84 %) in 2015 and to 145.41 km^2 (28.02 %) in 2020. In contract, *CL* and *FR* reduced from 69.40 km^2 (13.37 %) and 139.92 km^2 (26.96 %) in 2010, to 20.92 km^2 (4.03 %) and 116.41 km^2 (22.43 %) in 2015, and to 7.44 km^2 (1.43 %) and 126.51 km^2 (24.38 %) in 2020. The NDBI computation shows that the BU areas of Awka are increasing, with a maximum value of 0.328 in 2010, 0.530 in 2015, and 0.649 in 2020. The NDVI computation shows that green vegetation decreased from a maximum value of 0.728 in 2010 to 0.579 in 2015 and 0.537 in 2020. *BU* may have been rising in the study area as a result of migration, urbanization, and infrastructural development. It threatens the existence of *CL* and *FR* and is found to be a crucial driver of climate change and food insecurity in the study area. *CL* is essential to food security and the achievement of SDG 2. *FR* mitigates against climate change and food insecurity. It is crucial for the achievement of SDG 2, as it contributes directly and indirectly to food security and nutrition. From our study, we see that *BU* has been expanding while *CL* and *FR* decreased from 2010 to 2020. Following our study's findings and reports from the United Nations (UN, 2020), we simulate that by 2030 (10-year planning period), *BU will have* further increased in the study area. Since *BU* has been found to be a driving force behind *CL* and *FR* loss in the study area, we report that by 2030, *CL* and *FR* will further decrease in size. If *CL* and *FR* are simulated to reduce the size of the study area by 2030, then Awka will be facing challenges of food insecurity and climate change. Thus, if Awka seeks to address issues of food insecurity and mitigate against climate change in order to achieve SDGs 2 and 13 by 2030, it must adopt sustainable agriculture, practice forest regeneration techniques such as continuous cover forestry, and then ignite laws against the conversion of *CL* and *FR* to *BU* areas.

Table 8: Review that relates the study's findings with SDGs 13 and 2 output targets/indicators

(a) Review that relates the study's findings with SDG 13 output targets and its indicators

Output Targets	Indicators	Background Information
13.1 "Boost resiliency to withstand risks and adapt to natural disasters brought on by climate change."	**13.1.1** "Fatalities recorded, missing persons, and those directly influenced by disasters per 100,000 people."	Fatalities in Awka as a result of climate change can be traced to losses in *FR* and *CL* and an increase in the *BU* areas. Our classification results show that Awka's *FR* degraded from 139.92 km^2 in 2010 to 126.51 km^2 in 2020. The NDVI analysis further shows that green vegetation was degrading in the study area during the same period. If Awka intends to accomplish SDG 13 by 2030, it must rehabilitate its damaged forest. Rehabilitating its damaged forest will prove that Awka is resilient and capable of adapting to dangers arising from climate change.
	13.1.2 "Countries that enforce and implement measures to reduce the danger of natural disasters"	
	13.1.3 "Local councils that develop and implement disaster risk reduction measures that are in line with national plans"	
13.2 "Embrace national planning, strategies, and policies that address climate change."	**13.2.1** "Countries that have discussed the implementation of a common strategy, objective, or policy that increases their ability to adapt to the adverse effects of climate change, fosters climate resilience, and boasts greenhouse gas emissions without endangering food production"	The study's findings show that Awka's *FR* and *CL* have been decreasing. This decrease in Awka's *FR* is a crucial factor that contributes to the area's climate change. To mitigate against the effects of climate change, the study region must embrace national planning, strategies, and policies as measures to combat the effects of global warming.
13.3 "Boost institutional and individual capacity for tackling climate change through enlightenment, instruction, adaptation, damage mitigation, and early warning."	**13.3.1** "Countries whose school system curricula cover early warning, damage reduction, and mitigation"	Our final findings show that *FR* and *CL* are decreasing in the study area as a result of an increase in *BU*. Hence, *BU* is a driver of *FR* and *CL* losses. If Awka intends to meet SDG 13 by 2030, it must regenerate its degrading *FR* ecosystem by creating public awareness and enlightenment through educational, skill-building, and advocacy activities.
	13.3.2 "Countries whose structural, institutional, and individual efforts support initiatives for program assistance, technology transfer, mitigation, and development"	

(b) **Review that relates the study's findings with SDG 2 output targets and its indicators**		
Output Targets	**Indicators**	**Background Information**
2.1 By 2030, eradicate hunger and provide year-round access to safe, nourishing, and sufficient food for all, particularly the less privileged and vulnerable ones, including infants.	**2.1.1** "Prevalence of malnutrition" **2.1.2** "The percentage of people who experience moderate to severe food insecurity, as determined by the Food Security Survey".	*FR* and *CL* are crucial to achieving food security. The study's findings show that Awka is losing its *FR* and *CL*. *FR* and *CL* are found to decrease from 139.92 km^2 and 69.40 km^2 in 2010 to 126.51 km^2 and 7.44 km^2 in 2020. If Awka intends to accomplish SDG 2.1 by 2030, it must regenerate its *FR* areas and practice sustainable agriculture
2.2 By 2030, halt all forms of malnutrition by 2025, including meeting the goals for stunting and wasting in kids under the age of 5. In addition, take care of the nutrition of old, adolescent, pregnant, and breast-feeding mothers.	**2.2.2** "Prevalence of under nutrition, by type (wasting and overweight), in children under the age of 5" **2.2.3** "Prevalence of anemia among women within the age bracket of 15 to 49, stratified by pregnancy status (percentage)"	The study's final findings show that Awka is still behind in achieving goal 2.2 by 2025. Thus, if Awka is prepared to eliminate malnutrition by 2025, it must provide incentives to local farmers, invest in sustainable agriculture, and publish a stop notice to all forms of encroachment into *CL*.
2.3 By 2030, ensure the agricultural output and wages of artisanal food manufacturers, especially women, domestic peoples, subsistence farmers, fishermen, and pastoralists, by ensuring safe and fair access to land, productive resources and inputs, knowledge, markets, financial products and opportunities, and non-farm and value-added jobs	**2.3.1** "Production rate per worker unit by classes in agriculture, forestry, and pastoral enterprises" **2.3.2** "Median income of artisanal food manufacturers, given by sex and domestic status"	The loss in the study area's *FR* and *CL* shows that Awka is on the verge of achieving goal 2.3. Thus, if the study area intends to achieve target 2.3 by 2030, it must ensure that agricultural output and wages for artisanal food manufacturers are guaranteed.

CONCLUSION

The study used remotely sensed tools to map the LU changes in Awka from 2010 to 2020. Due to anthropogenic activities, Awka's LU classes have been experiencing changes in the last few decades. These LUC, which are driven mainly by an increase in built-up area, impact the city's forest and cultivated land areas, thereby leading to climate change and food insecurity. In this study, three remotely sensed satellite datasets (Landsat 7 ETM+ (2000) and Landsat 8 OLI (2015, 2020) were used to analyze the LU changes in Awka from 2010–2020. The ground-truth information was used for validation. The results show that from 2010 to 2015, built-up area increased from 98.56 km^2 (18.99 %) to 113.35 km^2 (21.84 %) and 145.42 km^2 (28.01 %), while cultivated land decreased from 69.40 km^2 (13.37 %) to 20.92 km^2 (4.03 %) and to 7.44 km^2 (1.43%) during the same period. Forest cover changed from 139.92 km^2 (26.96 %) in 2010 to 116.41 km^2 (22.43 %) and to 126.51 km^2 (24.38 %) in 2020. Water bodies, bare land, and grassland had also changed. Water bodies, grassland, and bare land areas changed from 7.05 km^2 (1.36 %), 99.79 km^2 (19.23 %), and 104.30 km^2 (20.10 %) in 2010 to 32.34 km^2 (6.23 %), 117.89 km^2 (22.71 %), and 118.11 km^2 (22.76 %) in 2015 and to 8.56 km^2 (1.65 %), 45.62 (8.79 %), and 185.48 km^2 (35.74 %) in 2020. The NDBI and NDVI computations show that built-up areas increased while areas of green vegetation decreased. From the computation, the NDBI analysis shows that built-up areas increased with a maximum value of 0.328 in 2010, 0.530 in 2015, and 0.649 in 2020, while the NDVI results show that green vegetation decreased with a maximum value of 0.728 in 2010, 0.579 in 2015, and 0.537 in 2020. The study shows that the city's LU classes are changing. These changes tend to have a detrimental impact on its cultivated land and forest cover, which are driven mainly by an increase in built-up areas. From the study, we see that the study area may be threatened by climate change and food insecurity. These threats may hinder the city from achieving SDGs 2 and 13. Thus, if the study area intends to achieve SDGs 2 and 13 by 2030, it must invest in agriculture and halt the exploitation of forest resources. It must practice tree regeneration and sustainable agricultural practices.

CONFLICT OF INTEREST

The authors declare that they have no competing interests.

REFERENCES

Abebe, G., Getachew, D., Ewunetu, A. (2022). Analyzing land use/land cover changes dynamics using remote sensing and GIS in Gubalafito district, Northeastern Ethiopia, SN *Applied Sciences*, 4(1), https://doi.org/10.1007/s42452-021-04915-a.

Abebe, M.S., Deribew, K.T. & Gemeda, D.O. (2019). Exploiting temporal spatial patterns of informal settlements using GIS and remote sensing technique: A case study of Jimma city, Southwestern Ethopia, *Environmental System Research*, 8(1). https//doi.org/10.1186/ s40068-019-0133-5.

Abraham, T., Tilashwork, C., Tesfaye, F. & Abdlesemad, J. (2016). Impact assessment of land use/land cover change on soil erosion and rural livelihood in andit tid watershed, North Shewa, Ethopia. *Archives of Current Research International*, 3(1), 1-10 https://doi.org/10.9734/ACRI/2016/22268.

Aderele, M., Bola, T.S., Oke, D.O. (2020). Land use/land cover changes of Ago-Owu Forest

reserve, Osun state, *Nigeria using remote sensing techniques*, 10(4), https://doi.org/10.4236/ojf.2020.104025.

Al-sharif, A.A. & Pradhan, B. (2013). Urban sprawl analysis of Tripoli Metropolitan city (Libya) using remote sensing data and multivariate logistic regression model. *J Indian Soc of Remote Sens:* 1-15, https://doi.org/10.1007/212524-013-02997.

Anderson, G.L., Hardy, E.E., Roach, J.R., Witmer, R.E. (1976). *A land use and land cover classification system for use with remote sensor data*, USGS Professional Paper, Washington, DC.

Appiah, J.O., Agyemang-Duah, W., Sobeng, A.K., Kpienbaareh, D. (2021). Analysing patterns of forest cover change and related land uses in the Tano-Offin forest reserve in Ghana: *Implications for forest policy and land management*, 5, https://doi.org/10.1016/j.tfp.2021.100105.

Ariti, A.T., Viliet, J.V., Verburg, P.H. (2015). Land-use and land-cover changes in the central rift valley of Ethiopia: In *Assessment of perception and adaptation of stakeholders*, 65 (p. 28-37), https:doi.org/10.1016/j.apgeog.2015.10.002.

Ayele, G.T., Tebeje, A.K., Demissie, S.S., Belete, M.A., Jemberrie, M.A., Teshome, W.M., & Teshale, E.Z. (2018). Time series land cover mapping and change detection analysis using geographic information system and remote sensing. *Northern Ethiopia. Air, Soil and Water Research*, 11, 1-18, https://doi.org/10.1177/1178622117751603.

Bazai, M.H. & Panezai, S. (2020). Assessment of urban sprawl and land use change dynamics through GIS and remote sensing in Quetta, Balochistan, Pakistan. *Journal of Geography and Social Sciences,* 2(1), 31-50, http://www.jgss.com.pk.

Bhatti, S.S. & Tripathi, N.K. (2014). Built-up area extraction using Landsat 8 OLI imagery. *GIScience & Remote Sensing*. 51(4), 445-467. https://doi.org/10.1080/15481603. 2014.939539.

Boschetti, L.,Flasse, S., & Brivio P. (2004). Analysis of the conflict between omission and commission in low spatial resolution dichotomic thematic products: the Pareto Boundary, *Remote Sens. Environ*. 91(3-4), 280–292. https://doi.org/10.1016/j.rse.2004.02.015.

Bradley, B.A. (2009). Accuracy Assessment of mixed land cover using a GIS–designed sampling scheme. *Int. J. Remote Sens*. 30 (13), 3515–3529. https://doi.org/10.1080 /01431160802562263.

Chakilu, G. & Moges, M., (2017). Assessing the land use/cover dynamics and its impact on the low flow of Gumara Watershed, *Upper Blue Nile Basin, Ethiopia. Hydrol Current Res*, 7, 2, https://doi.org/10.4172/2157-7587.1000268.

Chang, Y., Hou K., Li X, Zhang Y. & Chen P. (2018). Review of land use and land cover change rsearch progress IOP Conference Series. *Earth and Environmental Science* 113, https://doi.org/10.1088/1755-1315/113/1/012087.

Chew, C., Shah, R., Zuffada, C., Haji, G., Masters, D., & Mannucci, A.J. (2016). Demonstrating soil moisture remote sensing with observations from the UK, TechDemoSat-1 satellite mission, *Geosphysical Research Letters*, 43(1), 3317-3324, https://doi.org/10.1002/2016GL068189.

Congalton, R.G., & Green, K. (2019). *Assessing the accuracy of remotely sensed data principles and practices* (3rd ed.) CRC press. Taylor and Francis group, Boca Raton, FL, 159–171. https://doi.org/10.1201/9780429052729.

Congedo, L. (2020). *Semi-Automatic Classification Plugin Documentation Release* 7.9.5.1. User Manuel, August, 1 – 255.

Coppins, P., Jonekheere, I., Nackaerts, K., Muys, B. & Lambin E. (2004). Digital change detection methods in ecosystem monitoring: A review. INT. *J. of Remote Sensing*, 25(9), 1565–1596 https://doi.org/10.1080/0143116031000101675.

Dash, P.P., Kakkar, R., Shreenivas, V., Pradesh, P.J., Mythri, D.J., Singh, K.H.V., Singh, V.V. & Sahai, R.M.N. (2015). Quantification of urban expansion using geospatial technology. A case study in Bangalore. *Advance in Remote Sensing*, 4(4), 330-342, https://doi.org/10.4236/ars.2015.44027.

Disperati, L. and Virdis, S. (2015). Assessment of land-use and land-cover changes from 1965 to 2014 in Tam Giang-Cau Hai Lagoon, central Vietnam. *Applied Geography* 58, 48–64 https://doi.org/10.1016/j.apgeog.2014.12.012.

Enoh, M.A., Richard, E.N., Uzoma, C.O., (2022). *Modelling and mapping the spatial-temporal changes in land use and land cover in Lagos: A dynamics for building a sustainable urban city.* Adv Space Res, https://doi.org/10.1016/j.asr.2022.07.042.

Enoh, M.A., Okeke, U.C., Nkechi, B.C. (2023). Mapping and simulating the spatial-temporal changes in the Lagos wetland ecosystem: A step-by-step approach to creating a carbon-neutral sustainable urban city. *Ecological modelling*, 482, https://doi.org/10.1016/j.ecolmodel.2023.110399.

Esa, E, Assen, M, & Legass, A. (2018). Implications of land use/cover dynamics on soil erosion potential of agricultural watershed, northwestern highlands of Ethopia. *Environmental Systems Research*, 7(1). https://doi.org/10.1186/s40068-018-0122-0.

Ezenwaji, E. E., Okoye, A.C., & Awopeju, A.K. (2013). The relative contributions of climate elements and environmental factors to flooding in Awka urban area, *African Journal of Environmental Science and Technology*, 7(8), 808-814, https://doi.org/10.5897/ ajest2013.1519.

Ezenwaji, E.E., Phil-Eze, P.O., Enete, I.C. & Osuiwu, B.O. (2014). An analysis of the cycles and periodicities of annual rainfall over Awka region, Nigeria. *Atmospheric and Climate Sciences*, 4, 665-671. http://dx.doi.org/10.4236/acs.2014.44059.

Firdaus, R., Nakagoshi, N., & Idris, A. (2014). Sustainability assessment of Humid Tropical Watershed: A case of Batang Merao Watershed, Indonesia. *Procedia Environmental Sciences*, 20, 722-731. https//doi.org/10.1016/j.proenv.2014.03.085.

Forkel, M., Carvalhais, N., Verbesselt, J., Mahecha, M., Neigh, C. & Reichstein, M. (2013). Trend change detection in NDVI time series: Effects of inter-annual variability and methodology. *Remote Sensing*, 5(5), 2113-2144, https://doi.org/10.3390/rs5052113.

Fu, H., Shao Z., Fu P., & Cheng Q. (2017). The Dynamics analysis between urban nighttime economy and urbanization using DMSP/OLS nighttime light data in China from 1992 to 2012. *Remote Sens*. 9(5), 416. https://doi.org/10.3390/rs9050416.

Hc, H., Srikanth, L., & Surendra, H.J. (2020). Prioritization of sub-watersheds of the Kanakapura watershed in the Arkavathi River Basin, Kamataka, India using remote sensing and GIS. *Geology, Ecology, and Landscapes*, 5(2), 149-160, https://doi.org/10.1080 /24749508.2020.1846841.

Hegazy, I.R. & Kaloop, M.R.(2015). Monitoring urban growth and land use change detection with GIS and remote sensing techniques in Daqahlia governorate Egypt. International *Journal of Sustainability Built Environment*, 4(1), 117-124. https:doi.org/10.1016/j.ijsbe. 2015.02.005.

Islam, T., Sah, M., Baral S., and Roychoudhury, R. (2018). A Faster technique on rice

disease detection using image processing of affected area in agro-field. In *Proceedings of the 2nd International Conference on Inventive Communication and Computational Technologies (ICICCT)* (pp. 62 – 66). Coimbatore, https://doi.org/10.1109/ICICCT. 2018.8473322.

Khan, M.J, Zeeshan, M.M, & Ali, S.S. (2020). GIS-based change detection of coastal features along Karachi coast Pakistan, *Pakistan Journal of Science*, 72(2), 124.

Khan, N.M., Rastoskuev, V., Sato, Y. & Shiozawa, S. (2005). Assessment of hydro saline land degradation by using a simple approach of remote sensing indicators. *Agriculture Water Management*, 77 (1-3): 96-109, https://doi.org/10.1016/j.agwat.2004.09.038.

Kharazmi, R., Tavili, A., Rahdari, M.R., Chaban, L., Panidi, E. & Rodrigo-Comino, J. (2018). Monitoring and assessment of seasonal land cover changes using remote sensing. A 30-year (1987-2016) case study of Hamoun Wetland, Iran, *Environmental Monitoring and Assessment,* 190(6), 356, https://doi.org/10.1007/s10661-018-6726-z.

Kidane, M., Tolessa, T., Bezie, A., Kessete, N. & Endrias, M. (2019). Evaluating the impacts of climate change and land use/land cover (LU/LC) dynamics on the hydrological responses of the Upper Blue Nile in the Central Highlands of Ethiopia, *Spatial Information Research*, 27(2), 151-167, https://doi.org/10.1007/s41324-018-0222-y.

Landsat Project Science Office (2018). *Landsat 7 Science Data User's Handbook*. Goddard Space Flight Center, NASA, Wastingston, DC.

Langford, R.L. (2015). Temporal merging of remote sensing data to enhance spectral regolith, lithological and alteration patterns for regional mineral exploration. *Ore Geology Review*, 68, 14-29, https://doi.org/10.1016/j.oregeorev.2015.01.005.

Liu, C., Paul F., & Lalit K. (2007). Comparative Assessment of the measures of thematic classification accuracy. *Remote Sens. Environ*. 107(4), 606–616. https://doi.org/10.1016/j.rse .2006.10.010.

Malik, S.M., Arshad, S., Alam, K., & Bilal, O. (2020). Monitoring urban growth and land use changes using GIS and remote sensing: A case study of Tehsil Burewala. *Journal of Himalayan Earth Science*, 53(1), 140.

Mohammed, A.A., Shankar, K. & Hasan, R.N. (2019). Data on time series analysis of land surface temperature variation in response to vegetation indices in twelve Wereda of Ethopia using mono window, split window algorithm and spectral radiance model. *Data in Brief*, 27, 104773. https://doi.org/10.1016/j.dib.2019.104773.

Mohammady, M., Moradi, H.R., Zeinivand, H., & Temme, A. (2015). A comparison of supervised, unsupervised and synthesis land use classification methods in the North of Iran. *Int. J. Environ. Sci. Technol*. 12(5), 1515–1526, https://doi.org/10.1007/s13762-014-0728-3.

Mozumder, C. & Tripathi, N.K. (2014). Geospatial scenario based modelling of urban and agricultural intrusions in Ramsar wetland Deepor Beel in Northeast India using a multi-layer perceptron neural network. *International Journal of Applied Earth Observation and Geoinformation,* 32(1):92-104, https://doi.org/10.1016/j.jag.2014.03.002.

Msofe, N.K., Shang L., Lyimo, J. (2019). Land use change trends and their driving forces in the Kilombero valley floodplain, Southeastern Tanzania, *Sustainability*, 11(2), 505, https://doi.org/10.3390/su11020505.

National Population Commission (2013). *Nigeria Demographic and Health Survey (NDHS*), South East. Retrieved from dhsprogram.com/pubs/pdf/OF23/OF23SE.pdf.

Naz, A. & Rasheed, H. (2017). Modelling the rice land suitability using GIS and multi-criteria decision analysis approach in Sindh, Pakistan. *Journal of Basic and Applied*

Sciences, 13, 26-33, https://doi.org/10.6000/1927-5129.2017.1305.

Nzoiwu, C.P., Ezenwaji, E.E., Enete, I.C. & Igu, N.I. (2016). Analysis of trends in rainfall and water balance characteristics of Awka, *Nigeria*, 10(7), 186-196, https://doi.org/10.5897/jgrp2016.0603.

Osman, M.A.A., Abdel-Rahman, E.M., Onono, J.O., Otaka, L.A., Elhag, M.M., Adan, Tonnang, H.E. (2023). Mapping, intensities and future prediction of land use/land cover dynamics using google earth engine and CA-artificial neural network model. *PLoS ONE* 18(7):e0288694. https://doi.org/10.1371/journal.pone.0288694.

Pal, S. & Ziaul, S. (2017). Detection of land use and land cover change and land surface temperature in English Bazar urban centre. *Egypt Journal of Remote Sensing and Space Sciences*, 20(1), 125-145, https://doi.org/10.1016/j.ejrs.2016.11.003.

Parsa, A., Yavari, A. & Nejadi, A. (2016). Spatio-temporal analysis of land/land cover pattern changes in Arasbaran Biosphere Reserve: Iran. *Model Earth Syst. Environ*. 2, 1-13 https://doi.org/10.1007/s40808-016-0337-3.

Pontius, R.G., Shusas, E, & McEachern, M. (2004). Detecting important categorical land changes while accounting for persistence. *Agric. Ecosyst. Environment*. 101:251–268. https://doi.org/ 10.1016/j.agee.2003.09.008.

Radhakrishnan, N., Satish, K., Kumar, S. (2014). Analysis of urban sprawl pattern in Tiruchirappalli city using applications of remote sensing and GIS. *Arabian Journal Science and Engineering*, 39(7), 5555-5563. https://doi.org/10.1007/s13369-014-1099-2.

Rigden, A.J. & Li, D.(2017). Attribution of surface temperature anomalies induced by land use and land cover changes: Attribution of temperature anomalies, *Geophysical Research Letters,* 44(13), https://doi.org/10.1002/2017GL0738811.

Rawat, J.S. & Kumar, M. (2015). Monitoring Land/cover change using Remote Sensing and GIS Techniques: A case study of Hawalbagh Block, District Almora, Uttarakhand, India. *The Egyptian Journal of Remote Sensing and Space Science*, 18, 77-84. http://dx.doi.org/10.1016/j.ejrs.2015.02.002.

Rizvi, S.H., Fatima, H., Alam, K. & Iqbal, M.J. (2020). The surface urban heat island intensity and urban expansion: A comparison analysis for the coastal areas of Pakistan, Environment, *Development and Sustainability*, 23(4), 5520-5537. https://doi.org/10.1007/s10668-020-00828-5.

Romaguera, M., Vaughan, R.G., Ettema, J., Izquierdo-Verdiguier, E., Hecker, C.A. & Van der Meer, F.D. (2018). Detecting geothermal anomalies and evaluating LST geothermal component by combining thermal remote sensing time series and land surface model data. *Remote Sensing of Environment*, 204, 534-552, https://doi.org/10.1016/j.rse.2017.10.003.

Saleem, M., Ahmed, S.R., & Javed, M.A. (2020). Impact assessment of urban development patterns on land surface temperature by using remote sensing techniques: A case study of Lahore, Faisalabad and Multan district, *Environmental Science and Pollution Research*, 27(32), 39865-39878, https://doi.org/10.1007/s11356-020-10050-5.

Saifullah, K., Barus, B., & Rustiadi, E. (2017). Spatial modelling of land use/land cover change (LUCC) in South Tangerang city, Banten, IOP Conference Series: *Earth and Environmental Science*, 54(1), 1-12 https://doi.org/10.1088/1742-6596/755/1/011001.

Satir, O., Berberoglu, S., & Donmez, C. (2016). Mapping regional forest fire probability using artificial neural network model in a Mediterranean forest ecosystem. *Geomatics, Natural Hazards and Risk,* 7(5), 1645-1658, https://doi.org/10.1080/19475705.

2015.1084541.

Sewnet, A. (2015). Land use/cover change at infraz watershed, Northwestern Ethiopia. *Journal of Landscape Ecology*, 8(1), 69-83, https://doi.org/10.1515/jlecol-2015-0005.

Singh, P., Kikon, N, & Verma P. (2017). Impact of land use change and urbanization on urban heat island in Lucknow city, Central India. A remote sensing based estimate. *Sustain. Cities Soc*. 32, 100–114. https://doi.org/10.1016/j.scs.2017.02.018.

Singh, S.K., Mustak, S., Srivastava, P.K., Szaba, S., & Islam, T. (2015). Predicting spatial and Decadal LULC changes through Cellular Automata Markov Chain Models using Earth Observation datasets and Geo-information. *Environ. Process*, 2(1), 61–78.doi:10.1007/ s40710-015-0062-x.

Tariq, A., Siddiqul, S., Sharifi, A. & Shah, S. (2022). Impact of spatio-temporal land surface temperature on cropping pattern and land use and land cover changes using satellite imagery, Hafizabad District, Punjab Province of Pakistan. *Arabian Journal of Geosciences*, 15(11), 1045, https://doi.org/10.1007/s12517-022-10238-8.

Teferi, E., Bewket, W., Uhlenbrook, S., & Wenninger, J. (2013). Understanding recent land use and land cover dynamics in the source region of the Upper Blue Nile, Ethiopia: Spatially explicit statistical modeling of systematic transitions. *Agric. Ecosyst. Environ*. 165, 98–117. https://doi.org/10.1016/j.agee.2012.11.007.

Teshome, D.S., Moisa, M.B., Gemeda, D.O. & You, S. (2022). Effect of land use-land cover change on soil erosion and sediment yield in Muger Sub-Basin, Upper Blue Nile Basin, Ethiopia, *Land*, 11(12), 2173, https://doi.org/10.3390/land11122173.

UN, (2015). *Transforming our world: The 2030 Agenda for Sustainable Development*. Retrieved July 22, 2019, from https://sustainabledevelopment.un.org/post2015 /transformingourworld.

United Nations & Nations, U. (2015). Transforming our world. The 2030 agenda for Sustainable Development. In *General Assembly 70 session*. http://doi.org/10.1007/ s13398-014-0173-7.2.

Usman, U., Yelwa, S.A., Gulumbe, S.U. & Danbaba, A. (2013). Modelling relationship between NDVI and climate variables using Geographical Weighted Regression. American *Journal of Applied Mathematics and Statistics,* 1(5), 24-28, https://doi.org/10.12691 /ajams-1-5-3.

Verpoorter, C., Kutser, T., & Tranvik, L. (2012). Automated mapping of water bodies using Landsat multispectral data. *Limnology and Oceanography Methods*, 10(12), https://doi:10.4319/lom.2012.10.1037.

Wang, Z., Mao, D., Li, L., Jia, M., Dong, Z., Miao, Z., Ren, C., Song, C. (2015). Qunatifying changes in multiple ecosystem services during 1992-2002 in the Sanjiang Plain of China. *Sci. Total Environ.* 514, 119-130. https://doi:10.1016/j.scitotenv.2015.01.007.

Yirsaw, E., Wu, W., Shi, X., Ternesgen, H., & Bekeke, B. (2017). Land use/Land cover change modeling and the prediction of subsequent changes in Ecosystem Service values in a coastal area of China, the Su-Xi Chang region, *Sustainability*, 9(1204), 1-7, https://doi.org/10.3390/su9071204.

Yuan, T., Yiping, X., Lei, Z., & Danqing, L. (2015). Land use and cover change simulation and prediction in Hangzhou city based on CA-Markov Model. International Proceedings of Chemical, Biological and Environmental Engineering, 90(1), 108-113, https:doi.org/10.7763/IPCBEE.

Yuan, X., Longhui, L., Xi C, & Hao (2015). Effects of precipitation intensity and temperature

on NDVI-based grass change cover over Northern China during the period from 1982 to 2011. *Remote Sensing*, 7(8), 10164-10183, https://doi.org/10.3390/rs70810164.

Zainab N, Tariq A. & Siddiqul S. (2021). Development of Web-Based GIS alert system for informing environmental risk of Dengue infections in major cities of Pakistan, *Geosfera Indonesia,* 6(1), 77, https://doi.org/10.19184/geosi.v6i1.20792.

Zenebe, M., Berie, H.T., Woldeamanuel, T., Asfaw, Z., Kassa, H. (2018). Land use and land cover changes and the link to land degradation in Arsi Negele district, Central Rift Valley, *Ethiopia*, 12, 1-9, https://doi.org/10.1016/j.rsase.2018.07.012.

Zha, Y., Gao, J., Ni, S. (2003). Use of normalized difference built-up index in automatically mapping urban areas from TM imagery. *International Journal of Remote Sensing*, 24:583-594, https:doi.org/10.1080/01431160304987.

Zhou, W., Zhang, S., Yu, W., Wang, J., & Wang, W. (2017). *Effects of urban expansion on forest loss and fragmentation in six mega regions,* China. Remote Sensing, https://doi.org/10.3390/rs9100991.

Ziyad, A.A. & Prakash, S. (2020). A review paper on monitoring environmental consequences of land cover dynamics with the help of geo-informatics technologies. *Geosfera Indonesia*, 5(3), 364 – 377. https://doi.org/10.19184/geosi.v513.18284.

Zoungrana, B.J., Conrad, C., Thiel, M., Amekudzi, L.K. & Da E.D. (2018). MODIS NDVI trends and fractional land cover change for improved assessments of vegetation degradation in Burkina Faso, West Africa. *Journal of Arid Environments*, 153, 66-75. https://doi.org/10.1016/j.jaridenv.2018.01.005.

Zubair, M. & Javed, M. (2018). Land use detection using remote sensing and GIS (A case study of Rawalpindi Division) *American Journal of Remote Sensing*, 6(1), 39-51, https://doi.org/10.11648/j.airs.20180601.17.